Surface Chemistry at the Solid-Solid Interface; Selectivity and Activity in Mechanochemical Reactions on Surfaces

Resham Rana, Robert Bavisotto, Kaiming Hou, Nicholas Hopper, and Wilfred T Tysoe*[a]

This paper summarizes the concepts that underpin the way in which forces exerted on chemical systems can either accelerate their rates or induce reaction pathways that cannot be accessed thermally. This was first described in 1935 by Evans and Polanyi who showed how hydrostatic pressure could accelerate the rates of chemical reactions using a thermodynamic analysis of transition-state theory to demonstrate that the reaction rate increased exponentially with pressure, and depends on a so-called activation volume. This is typically ~17 Å^3/molecule and indicates that pressures on the order of GPa's are required to accelerate the rates of chemical reactions, which commonly occur at solid-solid interfaces such as found in a ball mill. We describe how surface mechanochemical reaction mechanisms are studied using the example of the shear-induced decomposition of carboxylates on copper. They thermally decompose on heating to ~650 K to evolve carbon dioxide and deposit a hydrocarbon on the surface but shear stresses accelerate the rate of this process so that it occurs at room temperature. However, it is also found that forces parallel to the COO plane induce a non-thermal reaction pathway to evolve carbon monoxide and adsorbed oxygen on the surface. This reaction pathway can be quenched by using adsorbed benzoate species because the larger area of the aryl ring accentuates the tilt of the COO plane towards the surface to increase the rate of the thermal reaction.

1. Introduction

Inducing chemical transformations using mechanical energy, the field of mechanochemistry, is one of the oldest synthetic strategies, with the earliest known examples tracing back to the Greeks three millennia ago,[2] and Michael Faraday worked in the field during the 19th century.[3] Despite its antiquity, and despite the large number of mechanochemical reactions that have been discovered empirically, some of which are discussed in this special collection, it still remains a challenge to predict the rates of even very simple mechanochemical reactions. This is, in part, due to the lack of simple model systems for which mechanochemical reaction pathways are known that would enable predictive theories to be developed. This paper briefly summarizes the concepts that underpin mechanochemistry and describes strategies than can be used to investigate surface mechanochemical reactions.

For the purposes of this paper, we define *molecular* mechanochemistry as experiments in which the reactant, known as a mechanophore, is stressed by exerting a force at specific points on the molecule using, for example, an atomic force microscopy (AFM) tip or optical tweezers.[4] This encompasses phenomena such as the behavior of molecular machines,[5] biological systems such as enzymes,[6] the operation of muscle fibers,[7] molecules for intracellular transport,[8] or to those with fluorescent properties that are modified by an imposed force.[9]

A perhaps more common application is *synthetic* mechanochemistry, the use of applied forces to accelerate reaction rates or to facilitate the syntheses of new materials. These reactions can often be carried out in the absence of a solvent and are therefore environmentally friendly, or "green" reactions.[4d,9a,10] Perhaps the most economically important and also the most environmentally relevant area of synthetic mechanochemistry is tribochemistry, in which beneficial films are formed on the rubbing surfaces of machines from mechanoactive molecules added to lubricants[11] to lower friction and wear and therefore minimize energy losses and the need for machinery repair.[12] For completeness, an important class of mechanical process should be mentioned in which there is no change in the system, but where energy is dissipated, which, in the case of solid-solid sliding manifests as a friction force, while it causes fluids to be viscous. The fundamental physical concepts that underpin mechanical energy dissipation, mechanochemistry and tribochemistry are the same[13] and have also been used to model other stress-induced processes such as dislocation motion,[14] material fracture[15] or earthquakes.[16]

Perhaps the first attempt to measure the pressure-induced acceleration of the rate of a chemical reaction was by Roentgen (of later X-ray fame),[17] but he was not able to impose sufficiently high pressures to measurably influence the reaction rate. However, measurable changes in the rates of pressure-induced reactions were subsequently found[18] and the first

[a] Dr. R. Rana, R. Bavisotto, Dr. K. Hou, N. Hopper, Prof. W. T Tysoe
Department of Chemistry and Biochemistry
University of Wisconsin-Milwaukee
Milwaukee, WI 53211 (USA)
E-mail: wtt@uwm.edu

This publication is part of a joint Special Collection of Chemistry—Methods and ChemSusChem including invited contributions focusing on "Methods and Applications in Mechanochemistry". Please visit chemistry-methods.org/collections to view all contributions.

theoretical analysis of mechanochemical reaction kinetics was by Evans and Polanyi based on a thermodynamic analysis of transition-state theory. The equilibrium constant of a reaction, K, depends on its change in Gibbs Free Energy, ΔG as:

$$\Delta G = -RTlnK$$

where R is the gas constant and T is the absolute temperature. Since $\Delta G = \Delta U + P\Delta V - T\Delta S$, the variation in equilibrium constant with (hydrostatic) pressure at a constant temperature is given by

$$\left.\frac{\partial lnK}{\partial P}\right|_T = -\frac{\Delta V}{RT},$$

where ΔV has the units of volume, and is interpreted as the volume change that occurs during the reaction. In 1935, Evans and Polanyi used the concepts of transition-state theory to describe the influence of an external potential f (this case, the hydrostatic pressure) on the rate of a chemical reaction[19] to derive the following equation:

$$\frac{dlnk}{df} = -\frac{(\alpha - \alpha')}{RT}$$

Here k is a rate constant and α and α' are factors such that $(\alpha - \alpha')f$ is the energy change of the system in passing from the initial to the transition state. For example, if $f = T$ then this becomes the Arrhenius equation. If $f = P$, the hydrostatic pressure, then

$$\left.\frac{\partial lnk}{\partial P}\right|_T = -\frac{\Delta V^{\neq}}{RT},$$

where $\Delta V^{\neq}$ is known as the activation volume and broadly corresponds to a volume change between the initial and transition states of the reaction. If the rate constant in the absence of an external pressure is k_0, the above equation can be easily integrated to give

$$k(P) = k_0 exp\left(\frac{P\Delta V^{\neq}}{RT}\right).$$

Interestingly, this has become known as the Bell equation by the molecular mechanochemistry community,[20] and was originally applied to analyzing cell adhesion. Since typical activation volumes are expected to be of the order of ~10 cm^3/mole (~17 $Å^3$/molecule), very high stresses (of the order of GPa) are required to induce significant changes in activation energy and thus in the reaction rate. While such large stresses are challenging to achieve, it turns out that they are commonly encountered in solid-solid contacts[21] so that mechanochemical reactions are often induced in a ball mill[22] or at a sliding interfaces in machines.[11a,b,d]

Experimental values of the activation volume have been used to provide information on the nature of the transition state[23] where the magnitude of $\Delta V^{\neq}$ relative to ΔV provided clues as to whether the transition state was "early" (i.e., reactant-like) or "late" (i.e., product-like).[24] Measurements of hydrostatic-pressure dependent activation volumes also provide a valuable resource of experimental results to compare with theory.[18]

Thus, it can be argued that mechanochemistry is largely a surface chemistry problem, although there are other methods of imposing high stresses,[25] and developing theoretical models to describe synthetic mechanochemical reaction rates will require understanding the reaction pathways occurring on surfaces under the influence of sliding forces. This is particularly challenging because commonly used surface analytical techniques cannot generally interrogate such buried solid-solid interfaces.[26]

Nevertheless, some progress has been made and the strategies to address this issue, further outlined below, use the thermal surface reaction pathways as a baseline for understanding the mechanisms, combined with first-principles density functional theory (DFT) analyses, to follow the reaction pathway during rubbing. Experiments are carried out in ultra-high vacuum (UHV) to prevent surface contamination as described in greater detail below. The reaction is followed by measuring the evolution of the surface composition as a function of the number of the times that the sample has been rubbed using spatially resolved surface analytical techniques such as Auger spectroscopy,[27] or by monitoring the gas-phase products formed during sliding using a sensitive mass spectrometer.[27a,28] The variation in friction coefficient can also be used as an in situ monitor of the rates of mechanochemical reactions.[29]

This approach was first illustrated by investigating the surface mechanochemical reaction pathways of dimethyl disulfide (DMDS) with copper.[30] This reaction is initiated by the formation of adsorbed methyl thiolates, which can react both thermally and tribochemically to form small, gas-phase hydrocarbons and deposit sulfur on the surface. The reaction proceeds by the initially perpendicular C–S bond tilting towards the surface to induce bond scission. The elementary-step kinetics have been used to describe the overall rate of formation of a lubricating film from a reaction between copper and DMDS vapor.[29b,30a] In this case, the rate of the thermal reaction is mechanochemically accelerated so that it occurs at room temperature, much lower than the ~450 K at which methyl thiolate thermally decomposes. Similar strategies have been used to demonstrate that the tribochemistry of borate esters is controlled by its initial thermal surface reaction pathways[31] and to identify the tribochemical reactions of phosphite esters on iron oxide.[32]

The approach is illustrated for the mechanochemical reactions of carboxylic acids on copper, which have been shown previously to adsorb at room temperature as a carboxylate species,[33] and are anchored strongly to the surface. The carboxylate structure is analogous to the adsorbed methyl thiolate species and the lowest-energy decomposition pathway occurs by the COO plane of the carboxylate species tilting towards the surface to induce C–COO bond cleavage to release CO_2,[29a] where the reaction rate is accelerated by the imposition

of both normal and shear (lateral) stresses.[30b] However, there are some key differences between the two reactions. First, the carboxylate species is more stable than the thiolate and decomposes on heating to ~650 K with an activation energy of 180 kJ/mol.[34] Second, the bidentate carboxylate species formed on copper[33] might be expected to react differently depending on the direction of the lateral force relative to the COO molecular plane; sliding perpendicular to the plane in the direction of the lowest-energy pathway may have a different influence than sliding parallel to it. This conjecture is investigated here by combining sliding experiments with first-principles quantum calculation to illustrate the types of mechanistic information that can be gleaned from such studies. The effect of changing the pseudo-cylindrically symmetric methyl group in the carboxylic acid (in acetic acid) to a planar phenyl group (in benzoic acid) is also investigated.

The surface chemistry of carboxylic acids on copper has been studied previously. Near-edge X-ray adsorption spectroscopy (NEXAFS) has been used to investigate the adsorption of a range of carboxylic acids on Cu(111), where the structure was found to depend on the chain length.[35] The deprotonation kinetics of carboxylic acids on copper have been investigated by using fluorine-modified chains[36] and studies on the decomposition of isotopically labeled carboxylic acids on copper have shown that the reaction is initiated by the removal of carbon dioxide from the carboxylate group.[37] Acetic acid has been found to be relatively thermally stable on Cu(110)[34] and decomposes by simultaneously desorbing carbon dioxide, methane and ketene at 650 K in temperature-programmed desorption (TPD). Some hydrogen evolves at ~300 K from COOH group deprotonation, and approximately 5% of the initial carbon remains on the surface after the completion of the reaction. Similarly, adsorbed benzoic acid has been found to be thermally stable on Cu(110) and decomposes by simultaneously desorbing carbon dioxide and benzene upon heating to 590 K in TPD.[38] It was found that the flat-lying benzoate species abstracts hydrogen atoms from adsorbed benzoate to release benzene with an activation energy of 29 kcal/mol.[39]

These molecules are also technologically relevant because long-chain carboxylic acids have been used as so-called boundary lubricants[40] in which a carboxylate self-assembled monolayer lowers friction by adsorbing strongly to the surface to prevent adhesion of the contacting interfaces.[41] The adsorbed carboxylic acids can also decompose under the influence of shear to form low-friction carbonaceous layers.[42] For example, low-friction films are formed from the reaction of functionalized fatty acids such as elaidic and oleic acid[42,43] on tetrahedral amorphous carbon. Molecular dynamics (MD) simulations of short-chain (~C_7) versions of these carboxylic acids reveal attachment of the carboxylic acid to one face of the contact via the –COOH functionality, with the simultaneous attachment of vinyl groups to the other face. The postulated formation of such molecular bridges results in large forces being exerted on the bridging carboxylic acid, which are proposed to facilitate its mechanochemical decomposition. Of particular interest is that the *cis* and *trans* conformations of these carboxylic acids show different tribochemical activities, likely because of steric constraints.[44]

The following compares the surface tribo/mechanochemical reaction pathways of acetic and benzoic acid on a copper foil, which is used rather than a single crystal because rubbing the surface with a tungsten carbide ball used as a counterface in the UHV experiments damages the surface so that the use of single-crystal samples would be prohibitively expensive. However, it has been shown that these clean and annealed copper foils exhibit sufficient order to display distinct low-energy electron diffraction (LEED) patterns indicating that the surface is ordered.[45]

Experimental and Theoretical Methods

Experiments were carried out in UHV chambers operating at pressures of $\sim 2.0\times10^{-10}$ Torr after bakeout. Infrared spectra were collected using a Bruker Vertex 70 infrared spectrometer using a liquid-nitrogen-cooled, mercury cadmium telluride detector,[46] which is relatively insensitive in the C–H stretching region of the spectrum. The complete light path was enclosed and purged with dry, CO_2-free air and spectra were collected for 1000 scans at 4 cm^{-1} resolution. The sample was exposed to acetic acid using a leak valve attached to the gas-handling line prior to collecting the infrared spectra and performing mechanochemical reactions. Benzoic acid was dosed using a Knudsen source and was placed inside a glass crucible wrapped with tantalum wire with a chromel/alumel thermocouple attached to sublime the benzoic acid. The sample temperature was monitored by means of a chromel/alumel thermocouple spot-welded to the edge of copper foil.

Mechanochemical experiments were also carried out in a UHV chamber operating at a base pressure of $\sim 2\times10^{-10}$ Torr following bakeout, which has been described in detail elsewhere.[47] Briefly, the sample was rubbed by a pin attached to a moveable arm in UHV while simultaneously measuring the normal load, lateral force and the electrical contact resistance between the tip and substrate. The arm was mounted to a rotatable Conflat flange to allow the pin to be rotated to face a cylindrical-mirror analyzer (CMA) to enable Auger spectra of the pin surface to be obtained.

All measurements were made using a sliding speed of $\sim 4\times10^{-3}$ m/s at a normal load of 0.44 N. Previous work has shown that the maximum interfacial temperature rise for a copper sample under these conditions is much less than 1 K[48] so that any changes found after rubbing the surface are not thermally induced. The spherical pin ($\sim 1.27\times10^{-2}$ m diameter) was made from tungsten carbide containing some cobalt binder and could be heated by electron bombardment, or by argon ion bombardment in order to clean it.

The copper foil was prepared by mechanical polishing using sandpapers of decreasing grit size until no visible scratches were observed. This was followed by polishing using polycrystalline diamond paste until a visibly smooth surface was seen under a microscope. The samples were mounted in UHV to a precision x, y, z manipulator for measuring the elemental profiles across a rubbed region of the sample. Auger spectra were either collected using the coaxial electron gun in the CMA with an electron beam energy of 3 kV, or with a Staib model EK050M2 Microfocus electron gun. The chamber is also equipped with a channeltron secondary electron detector which allowed scanning electron microscopy (SEM) images of the wear scar to be collected using the microfocus electron gun. Auger elemental profiles were obtained across the rubbed regions

to measure the loss of carbon or oxygen from the surface as a function of the number of times that the sample had been rubbed.

The copper foil sample was cleaned using a standard procedure consisting of Ar^+ bombardment with subsequent annealing to 850 K for 10 minutes. Ar^+ bombardment was performed at a background gas pressure of $\sim 5.0\times10^{-5}$ Torr at a 1 kV potential, while maintaining a ~2 μA sample current. This process was repeated until the sample was determined to be sufficiently clean by AES where, in particular, no carbon or oxygen were detected on the surface. Acetic (Sigma-Aldrich, >99.5% purity) and benzoic (Sigma-Aldrich, >99.5% purity) acids were purified using several freeze-pump-thaw cycles and the purity was judged by mass spectroscopy.

The adsorption geometry of acetic acid was calculated using periodic density functional theory (DFT) using the projector augmented wave (PAW) method as implemented in the Vienna ab-initio simulation package (VASP) code.[49] The exchange and correlation energies were calculated using the PBE3 (Perdew, Burke and Ernzerhof[50]) form of the generalized gradient approximation (GGA). The kinetic energy cutoff for all calculations was 400 eV. The wavefunctions and electron density were converged to within 1×10^{-5} eV whereas geometric structures were optimized until the forces on the atoms were less than 0.01 eV/Å. Van der Waals interactions were implemented using the DFT-D3 method as described by Grimme et al.[51] The reaction pathway and activation energy for acetate decomposition and for the rotational barrier of adsorbed benzoate on copper were measured using the climbing nudged-elastic band (NEB) method.[23]

2. Results

In order to confirm that acetate species form on a copper foil when dosed with acetic acid at room temperature,[52] infrared spectra were collected as a function of exposure and the results are displayed in Figure 1, where the background spectrum for the clean surface is also displayed. The spectra show an intense feature centered at 1437 cm^{-1} with a much less intense peak at 1028 cm^{-1}. These features have been identified previously for acetic acid adsorbed at room temperature on a Cu(100) surface[33] where the ν_s(COO) mode at 1437 cm^{-1} is associated with the formation of an acetate species and indicates that acetic acid has deprotonated on adsorption. The weak peak at 1028 cm^{-1} is due to a C–C stretching mode and, according to the surface selection rules,[53] its appearance suggests that the carbon-carbon bond is oriented with a component of the vibration being normal to the surface. Similarly, the corresponding asymmetric COO mode is completely absent indicating that the plane of the carboxylate group is oriented perpendicularly to the surface, in accord with the structure predicted by DFT.[1] This is structurally analogous to methyl thiolate species on copper[45] indicating that it should be susceptible to shear-induced decomposition by tilting towards the surface.

In order to test this, a clean copper sample was rubbed ~50 times to create a wear track and to stabilize the friction coefficient. Neither carbon nor oxygen were found on the surface after this procedure. The sample was then saturated with 2 L of acetic acid to form acetate species (Figure 1) and then rubbed with a tungsten carbide ball. The amount of carbon remaining within the rubbed region was measured using small-spot-size Auger spectroscopy as a function of the number of times that the sample had been rubbed. The results are shown in Figure 2 (■). The reduction in carbon Auger signal indicates that adsorbed acetate decomposes tribochemically. The exponential decay yields a value of the number of scans to reduce the amount of surface carbon to 1/e of its original amount, $S_e = 6.6 \pm 0.5$ scans. However, this procedure does not completely remove all carbon from the surface and the final C(KLL)/Cu(LMM) peak-to-peak Auger ratio after 25 scans is ~0.02 indicating that ~16% of the original carbon remains on the surface. This is significantly more than the ~5% carbon remaining after heating to ~650 K in a TPD experiment.[34] The relatively low intensity of the Cu Auger signal after the sample

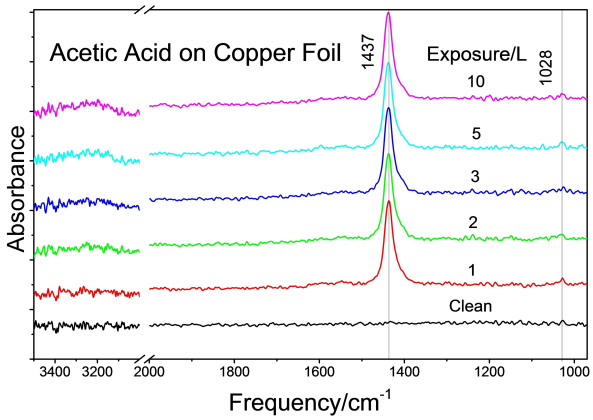

Figure 1. Infrared spectra of a copper foil dosed at room temperature with acetic acid as a function of exposure in Langmuirs (1 L (Langmuir) = 1×10^{-6} Torr s), where the exposures are displayed adjacent to the corresponding spectrum. Reprinted by permission from Springer from reference.[1]

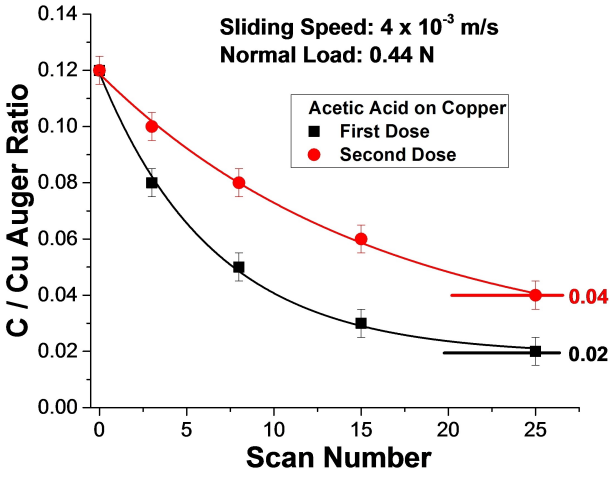

Figure 2. Plot of the ratio of the C(KLL) peak-to-peak Auger signal measured in the center of a wear track on a copper foil surface ratioed to the Cu(LMM) peak-to-peak signal from the substrate after the surface was dosed with 2 L of acetic acid as a function of the number of times that the sample had been rubbed at a load of 0.44 N and a sliding speed of 4×10^{-3} m/s. The results are shown for adsorption on a clean surface (■), and after redosing without cleaning the surface (●). Reprinted with permission from Ref. [1], Copyright 2021 Springer.

had been rubbed prohibited the lineshape from being used to identify the nature of the carbon on the surface. Note that attempts to measure the gas-phase products emitted into the chamber during rubbing were not successful in this case because of the small amount of residual acetic acid background in the chamber.

Figure 3 shows that the carbon removal is accompanied by the loss of oxygen from the surface where the number of passes to reduce the O(KLL)/Cu(LMM) ratio to 1/e of its original value, S_e, is 6.6 ± 0.8 scans, identical to the rate of loss of carbon (Figure 2), indicating that carbon and oxygen are removed simultaneously in the same tribologically induced reaction step. By measuring the relative carbon and oxygen Auger sensitivities

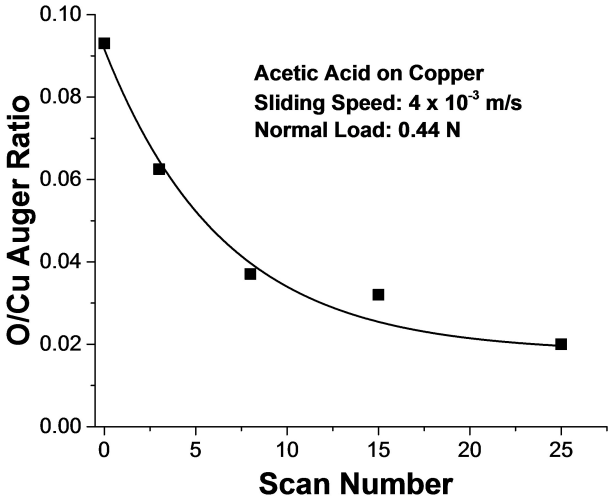

Figure 3. Plot of the ratio of the O(KLL) peak-to-peak Auger signal measured in the center of a wear track on a copper foil surface ratioed to the Cu(LMM) peak-to-peak signal from the substrate after the surface was dosed with 2 L of acetic acid as a function of the number of times that the sample had been rubbed at a load of 0.44 N and a sliding speed of 4×10^{-3} m/s. Reprinted with permission from Ref. [1], Copyright 2021 Springer.

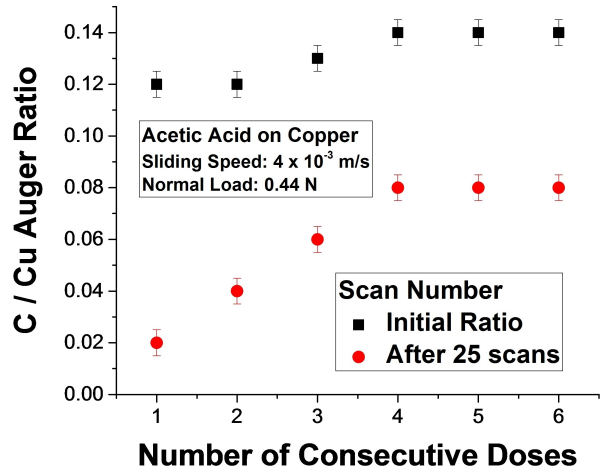

Figure 4. Plot of the initial (■) and final (●) C(KLL)/Cu(LMM) Auger ratios after 25 rubbing cycles for repeated dosing of the surface without cleaning the sample between doses. Experiments were performed at a load of 0.44 N and a sliding speed of 4×10^{-3} m/s. Reprinted with permission from Ref. [1], Copyright 2021 Springer.

of the Auger system used here by assuming a 1:1 C:O stoichiometry for the initially adsorbed acetate overlayer indicates that the carbon:oxygen stoichiometry of the remaining film is 0.8 ± 0.1.

During a mechanochemical reaction, which consists of continually dosing the surface while rubbing, the overall kinetics depends on how the surface composition evolves as the reaction proceeds. This is illustrated in Figure 2, which shows the effect of redosing a sample that was previously rubbed 25 times with acetic acid without any intervening cleaning (●). Now the mechanochemical reaction rate is slower (with S_e ~ 16 passes) than for the clean surface, and the amount of carbon on the surface doubles.

The effect of repeating this process is illustrated in Figure 4, which plots the C/Cu Auger ratio after exposing the sample to 2 L of acetic acid at room temperature before rubbing the sample (■) compared with the Auger signal after rubbing (●), as a function of the number of cycles. The data for the carbon coverage after rubbing (●) represent the amount of strongly bound carbon remaining on the surface after the reactive species have been removed. However, the surface can still accommodate acetate species and the difference between the upper and lower curves represents the proportion of the copper surface that contains available adsorption sites. The first two points for dose 1 and 2 are taken from the data shown in Figure 2, and the amount of carbon remaining on the surface after rubbing increases approximately linearly up to ~4 doses, and then remains constant, while the amount of carbon that can adsorb on the surface increases slightly. At larger dose-and-rub cycle, the values remain constant and the surface can adsorb ~50% of the initial acetate coverage on the clean surface. This indicates that the mechanochemical reaction selectivity increases as the surface becomes passivated so that the acetate species which initially adsorb on clean copper decompose tribochemically to remove a portion of the surface species, but the reaction causes some carbon and oxygen to be deposited onto the surface. As the coverage of decomposition products increases, the saturation coverage of the adsorbed acetates is reduced by ~50% and no detectable carbon is added to the surface. This implies that all the acetate species are mechanochemically removed and indicates that the film formation rate of the simple model carboxylic acid gas-phase lubricant is self-limiting. Presumably if the oxygen- and carbon-containing film is worn away, this would allow more acetate species to adsorb and repair the film.

In order to obtain insights into the pathway for the reaction of acetate species on copper, DFT calculations of acetate decomposition were performed using the nudged-elastic band method.[23] The energy profile for the lowest-energy acetate decomposition pathway is displayed in Figure 5. As indicated earlier, the reaction sequence is shown as insets to Figure 5 and shows that the reaction occurs by the plane of the adsorbed acetate species tilting so that the methyl group approaches the surface until the CH_3–C bond is weakened and ultimately breaks, resulting in the deposition of a methyl group on the surface and the elimination of carbon dioxide into the gas-phase. This will be referred to as in-plane tilt or the lowest-

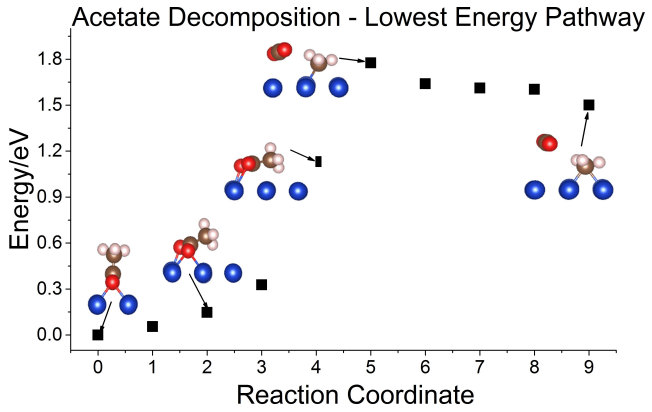

Figure 5. Reaction energy profile that plots energy versus the reaction coordinate for the lowest-energy pathway for the decomposition of acetate species on a Cu(100) slab obtained by using the nudged-elastic band method calculated using density functional theory. This reaction is initiated by a tilting perpendicular to the vertical OCO–CH_3 plane of the adsorbed acetate species to evolve carbon dioxide. Reprinted with permission from Ref. [1], Copyright 2021 Springer.

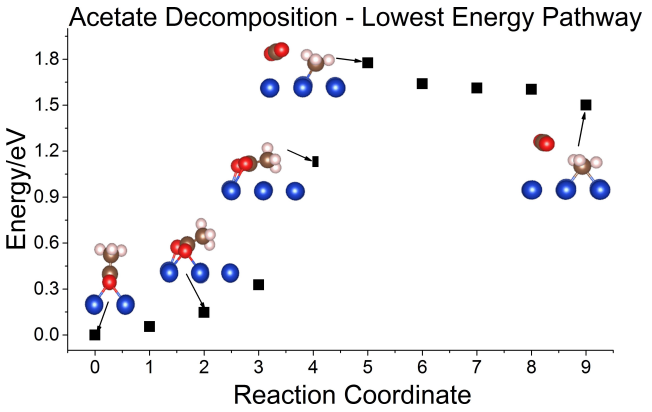

Figure 6. Reaction energy profile that plots energy versus the reaction coordinate for a high-energy pathway for the decomposition of acetate species on a Cu(100) slab obtained by using the nudged-elastic band method calculated using density functional theory. This reaction is initiated by a tilting within the vertical OCO–CH_3 plane of the adsorbed acetate species to evolve carbon monoxide and deposit atomic oxygen on the surface. Shown on the figure are depictions of how the structure evolves as the acetate species decomposes. Reprinted with permission from Ref. [1], Copyright 2021 Springer.

energy pathway. This reaction pathway is analogous to the methyl thiolate decomposition reaction except that the weaker C—S bond allows the reaction to occur at much lower temperatures than the acetate decomposition and the weak binding of CO_2 to the surface compared to sulfur results in it desorbing as it is formed. The calculated energy barrier is ~1.8 eV/molecule (173 kJ/mol), close to the value of 180 kJ/mol measured experimentally,[34] suggesting that the NEB calculations correctly reproduce the reaction pathway.

However, the thermal reaction deposits carbon, but no oxygen, while the mechanochemical reaction leaves a significant amount of oxygen on the surface (Figure 3). In order to investigate the possibility that this is due to other shear induced reactions, the reaction pathway and energy barrier were calculated for the acetate species tilting within the plane, perpendicular to the tilt direction for the lowest-energy pathway (Figure 5), and will be referred to as parallel tilt, or the higher-energy pathway. The results are shown in Figure 6, which also displays the evolution in structure as the reaction proceeds. Now the energy barrier increases to 2.5 eV (240 kJ/mol), somewhat higher than the lowest-energy pathway, as expected. Here, shear causes one of the carboxylate oxygens to detach from the surface to initially form an η^1-acetate species that continues to tilt as the reaction proceeds. This induces the formation of a bent $CO_2^{\delta-}$ species that has been detected on copper at high CO_2 pressures,[54] which reacts to form CO and adsorbed oxygen.

A similar series of experiments was carried out using benzoic acid, in which the methyl group of acetic acid is replaced by an aryl group. The results for the loss of carbon from the surface as a function of the number of rubbing cycles is shown in Figure 7 (■), where $S_e = 6.7 \pm 1.3$ scans, similar to the value found for acetic acid (Figure 2).

However, the amount of carbon remaining on the surface (with a C/Cu Auger ratio of 0.09) reflects the greater amount of carbon in the precursor molecule. The carbon deposited in the

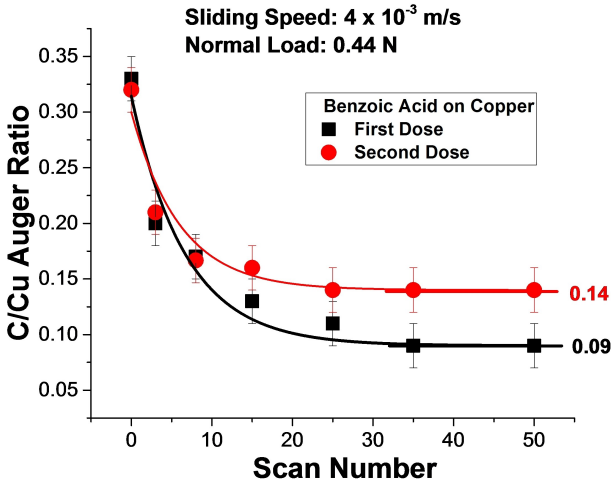

Figure 7. Plot of the ratio of the C(KLL) peak-to-peak Auger signal measured in the center of a wear track on a copper foil surface ratioed to the Cu(LMM) peak-to-peak signal from the substrate after the surface was dosed with 2 L of benzoic acid as a function of the number of times that the sample had been rubbed at a load of 0.44 N and a sliding speed of 4×10^{-3} m/s. The results are shown for adsorption on a clean surface (■), and after redosing without cleaning the surface (●).

second scan increases after rubbing, to a C/Cu Auger ratio of 0.14, but the rate of removal is essentially identical to that found in the first scan. The evolution of the oxygen Auger signal as a function of the number of scans is shown in Figure 8, where the initial oxygen coverage for benzoic acid is less than for acetic acid (with an O/Cu Auger ratio of 0.08 compared to 0.093 for acetate species on copper, Figure 3). However, in this case, the oxygen has been completely removed after ~35 scans, with $S_e = 9 \pm 2$ scans, with the same as the rate of the carbon removal (Figure 7).

The general behavior of benzoic acid on copper with increasing dose-and-rub cycles is the same as for acetic acid

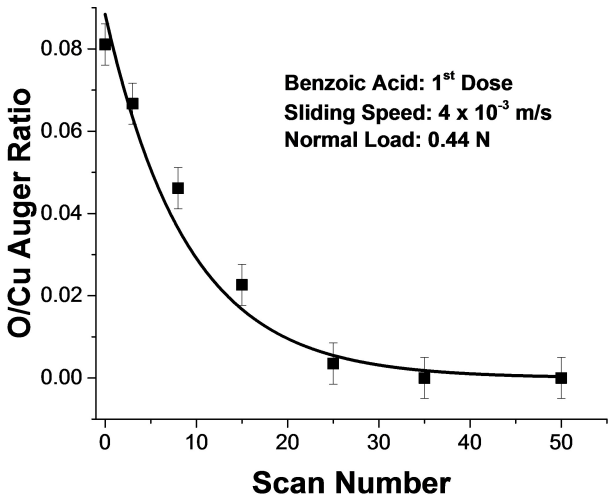

Figure 8. Plot of the ratio of the O(KLL) peak-to-peak Auger signal measured in the center of a wear track on a copper foil surface ratioed to the Cu(LMM) peak-to-peak signal from the substrate after the surface was dosed with 2 L of benzoic acid as a function of the number of times that the sample had been rubbed at a load of 0.44 N and a sliding speed of 4×10^{-3} m/s.

(Figure 9). The amount of carbon remaining on the surface after 50 scans increases with the number of rubbing cycles to form a stable overlayer with a C/Cu Auger ratio of ~0.18, about twice as high as the amount of carbon on a surface formed by acetate decomposition (Figure 4). However, while the total amount of carbon on the surface increases only slightly as the surface is dosed with benzoic acid after rubbing, there is a significant increase in the total amount of carbon that can be accommodated on the carbon-covered surface compared to the clean surface after several dosing and rubbing cycles with benzoic acid, where the C/Cu Auger ratio increase to ~0.47 compared to 0.33 for clean copper. This indicates that only a slightly lower coverage of benzoic acid (with a C/Cu Auger ratio of ~0.29) can adsorb on a surface with a C/Cu Auger ratio of ~0.18 as on the clean surface, where the saturated overlayer has a C/Cu Auger ratio of 0.33. This suggests the reactively formed carbonaceous layer, despite containing relatively more carbon than from a layer formed from acetate decomposition, still leaves a relatively high proportion of vacant adsorption sites.

Again, once the surface carbon coverage has attained a constant value, in this case, with a C/Cu ratio of ~0.18, the amount of carbon that can be adsorbed on the surface is about 90% of the initial carbon, and is all removed without depositing additional carbon.

The most striking difference between the tribochemistry of acetate and benzoate species on copper is that no oxygen is deposited from the decomposition of benzoate species (Figure 8) compared to the significant amount of oxygen that remains after acetate decomposition (Figure 3).

The DFT results suggest that the oxygen is formed from acetate decomposition due to the adsorbed acetate undergoing a parallel tilt caused by mechanical stress to form an η^1-acetate intermediate, which reacts to desorb CO and deposit oxygen on the surface (Figure 6). The planar geometry of an adsorbed benzoate species would be expected to result in a larger force being exerted to induce an in-plane tilt of the OCO group towards the surface as found for the thermal pathway (Figure 5). The force exerted in the orthogonal direction would be expected to be much lower and thus not be capable of inducing the higher-energy pathway, resulting in no oxygen being formed from the mechanochemical reaction. The validity of this postulate relies on the aryl ring being rigid enough not to rotate azimuthally, and this is investigated in Figure 10, which plots the variation in energy as a function of ring rotation obtained by NEB calculations The energies are plotted versus the rotation angle with the co-planar configuration ($\theta=0$ and 180°) being the most stable. As the ring rotates, the energy increases significantly to ~0.27 eV (~26 kJ/mol), indicating that the molecule is quite rigid.

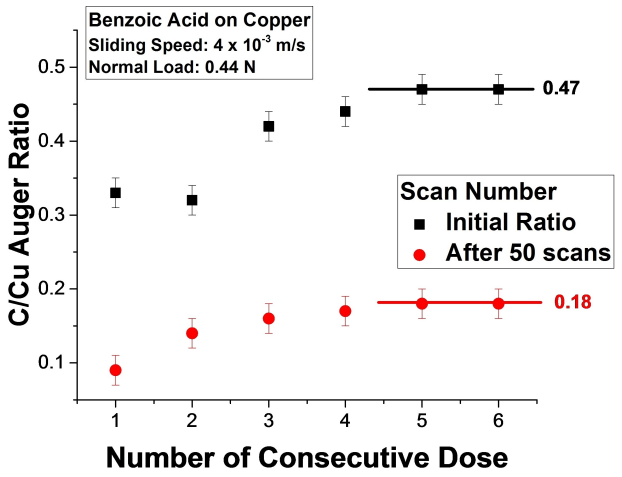

Figure 9. Plot of the initial (■) and final (●) C(KLL)/Cu(LMM) Auger ratios after 25 rubbing cycles for repeated dosing of the surface with benzoic acid without cleaning the sample between doses. Experiments were performed at a load of 0.44 N and a sliding speed of 4×10^{-3} m/s.

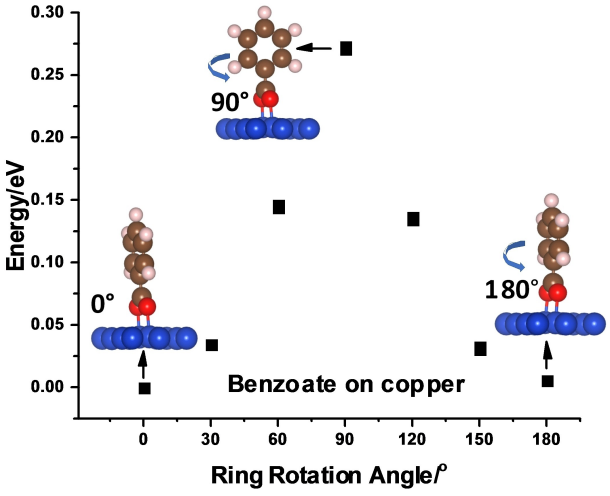

Figure 10. Energy variation for benzoate species on a Cu(100) slab obtained by using density functional theory as a function of azimuthal rotation angle of the aryl ring with respect to the adsorbed acetate species. Shown on the figure are depictions of how the structure varies with rotation angle.

3. Discussion

Carboxylic acids, including acetic and benzoic acid, deprotonate to form η^2-carboxylates when adsorbed on copper at room temperature with the oxygen atoms bound to copper bridge-site atoms as evidenced by infrared spectroscopy (Figure1) and DFT calculations (Figures 5, 6 and 10), in a behavior typical of the chemistry of carboxylic acids on transition-metal surfaces.[52] The structure involves the C–COO bond of the methyl and aryl groups being perpendicular to the surface. The lowest-energy barrier calculated for carboxylate decomposition is ~173 kJ/mol (Figure 5), consistent with the temperature at which carbon dioxide evolves from copper in TPD.[34,52,55] This lowest-energy decomposition pathway involves a molecular in-plane tilt towards the surface (Figure 5) to induce C–C bond scission to evolve carbon dioxide. Ketene is also formed from acetate decomposition.[34]

While the thermal reaction occurs at ~650 K,[34,55–56] sliding induces a reaction at room temperature to remove carbon (Figure 2) and oxygen (Figure 3) from the surface with identical first-order rate constants by reducing the energy barrier so that the reaction proceeds relatively rapidly at ~290 K.[13h] However, the thermal reaction removes all oxygen, while some oxygen remains after the tribochemical reaction is complete (Figure 3).[34] This suggests an alternative reaction pathway due to lateral stresses cause a parallel tilt of the adsorbed acetate, which induces the formation of monodentate acetate species, which decompose to form CO and adsorbed oxygen via a bent $CO_2^{\delta-}$ intermediate (Figure 6),[54] where the barrier is slightly higher than for the thermal pathway.

Since the acetate species has pseudo cylindrical symmetry with a randomly azimuthally oriented carboxylate group, the forces parallel and perpendicular to the adsorbed carboxylate will be the same, giving rise to a reaction in which carbon dioxide is formed both by the lowest-energy pathway (with selectivity of ~60%, Figure 3) and another higher-activation-barrier process with a selectivity of ~40% to produce CO and deposit oxygen on the surface (Figure 6). This predicts that an adsorbed benzoate should have different forces exerted in a direction perpendicular to the aryl ring than parallel to it. Since the ring is co-planar with the carboxylate group, and since the azimuthal rotational barrier is quite high (Figure 10), the tribochemical reaction is expected to occur predominantly via an in-plane tilt to induce the lowest-energy pathway to remove carbon (Figure 7), but, more importantly, to remove all oxygen (Figure 8). This reaction leaves more carbon on the surface than does the decomposition of adsorbed acetate species, reflecting the larger amount of carbon in an aryl group than a methyl group. Curiously, the limiting carbonaceous layer coverage (with a C/Cu Auger ratio of ~0.18) formed on the surface after ~5 dose-and-rub cycles (Figure 9) can adsorb almost the same coverage of benzoate species, as indicated by the difference between the initial C/Cu ratio (■) and the ratio after 50 scans (●), despite there being fewer exposed copper sites on the surface. In contrast, significant site blocking was induced by the carbon formed by the mechanochemical decomposition of acetate species (Figure 4). Although the total amount of surface carbon did increase slightly, presumably because of the higher carbon density in the reactively formed layer than for the adsorbed acetate (Figure 4), the effect is much larger for adsorbed benzoates (Figure 9).

Repeatedly adsorbing acetic acid on copper and rubbing results in the accumulation of carbon that produces a stable, low-friction film (Figure 4). At this point, the surface can accommodate only ~50% of the acetate species found on clean copper. This indicates that the tribochemical reaction of acetic acid with copper forms a self-limiting, lubricious film that contains both carbon and oxygen.

4. Conclusion

This paper illustrates the strategies that can be used to interrogate the chemistry induced by a mechanical force occurring at a sliding solid-solid interface by carrying out in situ experiments in ultrahigh vacuum and by comparing the results with the thermal chemistry found for the same system, and by testing the validity of the proposed mechanisms using first-principles DFT calculations. The results show that thermal reactions that would not normally occur until heating to over 600 K can be induced by rubbing under relatively mild conditions where the contact stress is estimated to be between 0.1 and 0.4 GPa.[29a] The decomposition of both benzoate and acetate species adsorbed on copper are induced at room temperature, where the adsorbate completely decomposed after ~30 rubbing cycles. The subsequent reaction pathway of the mechanically formed hydrocarbon fragment will also be different from the thermal reaction because of the different temperatures at which the fragments are generated, ~300 K for the mechanochemical reaction versus ~650 K for the thermal decomposition of carboxylates or ~450 K for thiolates.[45] This suggests that there are two effects that can influence mechanochemical reaction pathways; the intrinsic influence of the direction and magnitude of the imposed stress, and the different temperatures at which the reaction products are formed mechanically compared to the thermal reaction pathway.

A comparison of the reactions rates of methyl- and aryl-containing carboxylic acids, where the acetate decomposes via two distinct pathways depending on the direction of the force, while the benzoate decomposed via one pathway because of the asymmetry of the aryl ring, illustrates how the molecular structures can be tuned to influence the mechanochemical selectivity.

Finally, the mechanistic insights found for the mechanochemical reaction pathways of these simple model systems can form the basis for predictive, molecular-scale models for mechanochemical reactions that can eventually be applied to more complex systems or more severe conditions. It can be anticipated that, even if predictive models cannot be developed for more complex reactions, the principles developed by studying simple model systems will provide insights for designing and understanding more complex ones.

Acknowledgements

We gratefully acknowledge the Civil, Mechanical and Manufacturing Innovation (CMMI) Division of the National Science Foundation under grant number CMMI-2020525 for support of this work.

Conflict of Interest

The authors declare no conflict of interest.

Keywords: acetic acid · Cu(100) · infrared spectroscopy · density functional theory calculations · mechanochemistry · tribochemistry

[1] R. Rana, R. Bavisotto, N. Hopper, W. T. Tysoe, *Tribol. Lett.* **2021**, *69*, 32.
[2] H. J. Theophrastus, Theophrastus's history of stones : with an English version, and critical and philosophical notes, including the modern history of the gems, &c., described by that author, and of many other of the native fossils, London, **1774**.
[3] M. M. J. K. Faraday, Chemical manipulation : being instructions to students in chemistry on the methods of performing experiments of demonstration or of research with accuracy and success, Carey and Lea, Philadelphia, **1831**.
[4] a) J. J. Gilman, *Science* **1996**, *274*, 65; b) F. K. Urakaev, V. V. Boldyrev, *Powder Technol.* **2000**, *107*, 93–107; c) F. K. Urakaev, V. V. Boldyrev, *Powder Technol.* **2000**, *107*, 197–206; d) M. K. Beyer, H. Clausen-Schaumann, *Chem. Rev.* **2005**, *105*, 2921–2948; e) D. A. Davis, A. Hamilton, J. Yang, L. D. Cremar, D. Van Gough, S. L. Potisek, M. T. Ong, P. V. Braun, T. J. Martínez, S. R. White, J. S. Moore, N. R. Sottos, *Nature* **2009**, *459*, 68–72; f) H. M. Klukovich, T. B. Kouznetsova, Z. S. Kean, J. M. Lenhardt, S. L. Craig, *Nat. Chem.* **2013**, *5*, 110–114; g) J. R. Felts, A. J. Oyer, S. C. Hernández, K. E. Whitener Jr, J. T. Robinson, S. G. Walton, P. E. Sheehan, *Nat. Commun.* **2015**, *6*; h) P. Seema, J. Behler, D. Marx, *Phys. Chem. Chem. Phys.* **2013**, *15*, 16001–16011.
[5] P. Reimann, *Phys. Rep.* **2002**, *361*, 57–265.
[6] P. D. Boyer, *Annu. Rev. Biochem.* **1997**, *66*, 717–749.
[7] a) H. M. Lacker, C. S. Peskin, *Lect. Math. Life Sci.* **1986**, *16*, 32; b) A. F. Huxley, *Prog. Biophys. Biophys. Chem.* **1957**, *7*, 255–318.
[8] a) H. Khataee, A. Wee-Chung Liew, *Bioinformatics* **2013**, *30*, 353–359; b) K. Sasaki, M. Kaya, H. Higuchi, *Biophys. J.* **2018**, *115*, 1981–1992.
[9] a) S. L. Craig, *Nature* **2012**, *487*, 176–177; b) Z. Ma, F. Yang, Z. Wang, X. Jia, *Tetrahedron Lett.* **2015**, *56*, 393–396; c) T. Kosuge, X. Zhu, V. M. Lau, D. Aoki, T. J. Martinez, J. S. Moore, H. Otsuka, *J. Am. Chem. Soc.* **2019**, *141*, 1898–1902.
[10] a) J. Sohma, *Prog. Polym. Sci.* **1989**, *14*, 451–596; b) V. V. Boldyrev, K. Tkáčová, *J. Mater. Synth. Process.* **2000**, *8*, 121–132; c) C. Suryanarayana, *Prog. Mater. Sci.* **2001**, *46*, 1–184; d) V. I. Levitas, *Phys. Rev. B* **2004**, *70*, 184118; e) S. Kipp, V. Šepelák, K. D. Becker, *Chem. Unserer Zeit* **2005**, *39*, 384–392; f) Z. V. Todres, *Organic mechanochemistry and its practical applications*, Taylor&Francis, Boca Raton, FL, **2006**; g) B. M. Rosen, V. Percec, *Nature* **2007**, *446*, 381–382; h) S. A. Mitchenko, *Theor. Exp. Chem.* **2007**, *43*, 211–228; i) R. S. Varma, *Green Chem. Lett. Rev.* **2007**, *1*, 37–45; j) C. R. Hickenboth, J. S. Moore, S. R. White, N. R. Sottos, J. Baudry, S. R. Wilson, *Nature* **2007**, *446*, 423–427; k) J. Ribas-Arino, M. Shiga, D. Marx, *Angew. Chem. Int. Ed.* **2009**, *48*, 4190–4193; *Angew. Chem.* **2009**, *121*, 4254–4257; l) S. M. Hick, C. Griebel, D. T. Restrepo, J. H. Truitt, E. J. Buker, C. Bylda, R. G. Blair, *Green Chem.* **2010**, *12*, 468–474; m) J. Ribas-Arino, D. Marx, *Chem. Rev.* **2012**, *112*, 5412–5487; n) S. L. James, C. J. Adams, C. Bolm, D. Braga, P. Collier, T. Friscic, F. Grepioni, K. D. M. Harris, G. Hyett, W. Jones, A. Krebs, J. Mack, L. Maini, A. G. Orpen, I. P. Parkin, W. C. Shearouse, J. W. Steed, D. C. Waddell, *Chem. Soc. Rev.* **2012**, *41*, 413–447; o) R. Boulatov, *Nat. Chem.* **2013**, *5*, 84–86; p) G. A. Bowmaker, *Chem. Commun.* **2013**, *49*, 334–348.
[11] a) N. N. Gosvami, J. A. Bares, F. Mangolini, A. R. Konicek, D. G. Yablon, R. W. Carpick, *Science* **2015**, *348*, 102–106; b) J. Zhang, H. Spikes, *Tribol. Lett.* **2016**, *63*, 1–15; c) R. P. Glovnea, A. K. Forrest, A. V. Olver, H. A. Spikes, *Tribol. Lett.* **2003**, *15*, 217–230; d) N. J. Mosey, T. K. Woo, M. Kasrai, P. R. Norton, G. M. Bancroft, M. H. Müser, *Tribol. Lett.* **2006**, *24*, 105–114.
[12] K. Holmberg, P. Andersson, A. Erdemir, *Tribol. Int.* **2012**, *47*, 221–234.
[13] a) H. Spikes, W. Tysoe, *Tribol. Lett.* **2015**, *59*, 1–14; b) L. Prandtl, *Z. Angew. Math. Mech.* **1928**, *8*, 85; c) O. J. Furlong, S. J. Manzi, V. D. Pereyra, V. Bustos, W. T. Tysoe, *Tribol. Lett.* **2010**, *39*, 177–180; d) M. Müser, *Phys. Rev. B* **2011**, *84*, 125419; e) V. L. Popov, J. A. T. Gray, *Z. Angew. Math. Mech.* **2012**, *92*, 683–708; f) E. Gnecco, R. Roth, A. Baratoff, *Phys. Rev. B* **2012**, *86*, 035443; g) O. Furlong, S. Manzi, A. Martini, W. Tysoe, *Tribol. Lett.* **2015**, *60*, 1–9; h) W. Tysoe, *Tribol. Lett.* **2017**, *65*, 48; i) W. Kauzmann, H. Eyring, *J. Am. Chem. Soc.* **1940**, *62*, 3113–3125.
[14] a) G. B. Gibbs, *Phys. Status Solidi B* **1965**, *10*, 507–512; b) J. P. Hirth, W. D. Nix, *Phys. Status Solidi B* **1969**, *35*, 177–188.
[15] S. N. Zhurkov, *Int. J. Fract. Mech.* **1965**, *1*, 11.
[16] J. R. Rice, *Pure Appl. Geophys.* **1983**, *121*, 443–475.
[17] W. C. Röntgen, *Ann. Phys.* **1892**, *281*, 98–107.
[18] a) T. Asano, W. J. Le Noble, *Chem. Rev.* **1978**, *78*, 407–489; b) A. Drljaca, C. D. Hubbard, R. van Eldik, T. Asano, M. V. Basilevsky, W. J. le Noble, *Chem. Rev.* **1998**, *98*, 2167–2290.
[19] a) M. G. Evans, M. Polanyi, *Trans. Faraday Soc.* **1935**, *31*, 875–894; b) M. G. Evans, M. Polanyi, *Trans. Faraday Soc.* **1936**, *32*, 1333–1360.
[20] G. Bell, *Science* **1978**, *200*, 618–627.
[21] M. H. Müser, W. B. Dapp, R. Bugnicourt, P. Sainsot, N. Lesaffre, T. A. Lubrecht, B. N. J. Persson, K. Harris, A. Bennett, K. Schulze, S. Rohde, P. Ifju, W. G. Sawyer, T. Angelini, H. Ashtari Esfahani, M. Kadkhodaei, S. Akbarzadeh, J.-J. Wu, G. Vorlaufer, A. Vernes, S. Solhjoo, A. I. Vakis, R. L. Jackson, Y. Xu, J. Streator, A. Rostami, D. Dini, S. Medina, G. Carbone, F. Bottiglione, L. Afferrante, J. Monti, L. Pastewka, M. O. Robbins, J. A. Greenwood, *Tribol. Lett.* **2017**, *65*, 118.
[22] C. C. Piras, S. Fernández-Prieto, W. M. De Borggraeve, *Nanoscale Adv.* **2019**, *1*, 937–947.
[23] a) G. Henkelman, B. P. Uberuaga, H. Jónsson, *J. Chem. Phys.* **2000**, *113*, 9901–9904; b) G. Henkelman, H. Jónsson, *J. Chem. Phys.* **2000**, *113*, 9978–9985.
[24] C. A. Eckert, *Ann. Rev. Phys. Chem.* **1972**, *23*, 239–264.
[25] G. Cravotto, E. C. Gaudino, P. Cintas, *Chem. Soc. Rev.* **2013**, *42*, 7521–7534.
[26] W. G. Sawyer, K. J. Wahl, *MRS Bull.* **2008**, *33*, 1145–1150.
[27] a) O. J. Furlong, B. P. Miller, P. Kotvis, W. T. Tysoe, *ACS Appl. Mater. Interfaces* **2011**, *3*, 795–800; b) O. Furlong, B. Miller, W. Tysoe, *Tribol. Lett.* **2011**, *41*, 257–261; c) O. Furlong, B. Miller, W. T. Tysoe, *Wear* **2012**, *274–275*, 183–187.
[28] B. Miller, O. Furlong, W. Tysoe, *Tribol. Lett.* **2013**, *49*, 39–46.
[29] a) H. L. Adams, M. T. Garvey, U. S. Ramasamy, Z. Ye, A. Martini, W. T. Tysoe, *J. Phys. Chem. C* **2015**, *119*, 7115–7123; b) H. Adams, B. P. Miller, P. V. Kotvis, O. J. Furlong, A. Martini, W. T. Tysoe, *Tribol. Lett.* **2016**, *62*, 1–9.
[30] a) H. Adams, B. P. Miller, O. J. Furlong, M. Fantauzzi, G. Navarra, A. Rossi, Y. Xu, P. V. Kotvis, W. T. Tysoe, *ACS Appl. Mater. Interfaces* **2017**, *9*, 26531–26538; b) A. Boscoboinik, D. Olson, H. Adams, N. Hopper, W. T. Tysoe, *Chem. Commun.* **2020**, *56*, 7730–7733.
[31] a) B. P. Miller, O. J. Furlong, W. T. Tysoe, *Langmuir* **2012**, *28*, 6322–6327; b) B. Miller, P. Kotvis, O. Furlong, W. Tysoe, *Tribol. Lett.* **2013**, *49*, 21–29.
[32] R. Rana, W. Tysoe, *Tribol. Lett.* **2019**, *67*, 93.
[33] B. A. Sexton, *Chem. Phys. Lett.* **1979**, *65*, 469–471.
[34] M. Bowker, R. J. Madix, *Appl. Surf. Sci.* **1981**, *8*, 299–317.
[35] a) D. Fuhrmann, D. Wacker, K. Weiss, K. Hermann, M. Witko, C. Woll, *J. Chem. Phys.* **1998**, *108*, 2651–2658; b) M. Wühn, J. Weckesser, C. Wöll, *Langmuir* **2001**, *17*, 7605–7612.
[36] B. Immaraporn, P. Ye, A. J. Gellman, *J. Phys. Chem. B* **2004**, *108*, 3504–3511.
[37] B. Karagoz, A. Reinicker, A. J. Gellman, *Langmuir* **2019**, *35*, 2925–2933.
[38] J. Lee, O. Kuzmych, J. T. Yates Jr, *Surf. Sci.* **2005**, *582*, 117–124.
[39] a) J. Lee, D. B. Dougherty, J. T. Yates, *J. Phys. Chem. B* **2006**, *110*, 9939–9946; b) J. Lee, D. B. Dougherty, J. T. Yates, *J. Am. Chem. Soc.* **2006**, *128*, 6008–6009.
[40] a) D. Clayton, *Br. J. Appl. Phys.* **1951**, *2*, 25; b) F. J. Westlake, A. Cameron, *P. I. Mech. Eng., Conference Proceedings* **1967**, *182*, 75–78; c) A. Tonck, J. M. Martin, P. Kapsa, J. M. Georges, *Tribol. Int.* **1979**, *12*, 209–213; d) S. M. Hsu, R. S. Gates, *Tribol. Int.* **2005**, *38*, 305–312; e) H. Spikes, *Tribol. Lett.* **2015**, *60*, 5.
[41] R. Simič, M. Kalin, *Appl. Surf. Sci.* **2013**, *283*, 460–470.
[42] a) M. Kano, J. M. Martin, K. Yoshida, M. I. De Barros Bouchet, *Friction* **2014**, *2*, 156–163; b) M. I. De Barros Bouchet, J. M. Martin, J. Avila, M. Kano, K. Yoshida, T. Tsuruda, S. Bai, Y. Higuchi, N. Ozawa, M. Kubo, M. C.

Asensio, *Sci. Rep.* **2017**, *7*, 46394; c) M. I. De Barros Bouchet, J. M. Martin, C. Forest, T. le Mogne, M. Mazarin, J. Avila, M. C. Asensio, G. L. Fisher, *RSC Adv.* **2017**, *7*, 33120–33131; d) S. Campen, J. H. Green, G. D. Lamb, H. A. Spikes, *Tribol. Lett.* **2015**, *57*, 18.
[43] S. M. Lundgren, M. Ruths, K. Danerlöv, K. Persson, *J. Colloid Interface Sci.* **2008**, *326*, 530–536.
[44] T. Kuwahara, P. A. Romero, S. Makowski, V. Weihnacht, G. Moras, M. Moseler, *Nat. Commun.* **2019**, *10*, 151.
[45] O. J. Furlong, B. P. Miller, Z. Li, J. Walker, L. Burkholder, W. T. Tysoe, *Langmuir* **2010**, *26*, 16375–16380.
[46] M. Kaltchev, A. W. Thompson, W. T. Tysoe, *Surf. Sci.* **1997**, *391*, 145–149.
[47] F. Gao, O. Furlong, P. V. Kotvis, W. T. Tysoe, *Tribol. Lett.* **2008**, *31*, 99–106.
[48] O. J. Furlong, B. P. Miller, W. T. Tysoe, *Tribol. Lett.* **2011**, *41*, 257–261.
[49] a) G. Kresse, J. Hafner, *Phys. Rev. B* **1993**, *47*, 558–561; b) G. Kresse, J. Furthmüller, *Comput. Mater. Sci.* **1996**, *6*, 15–50; c) G. Kresse, J. Furthmüller, *Phys. Rev. B* **1996**, *54*, 11169–11186.
[50] J. P. Perdew, K. Burke, M. Ernzerhof, *Phys. Rev. Lett.* **1996**, *77*, 3865.
[51] S. Grimme, J. Antony, S. Ehrlich, H. Krieg, *J. Chem. Phys.* **2010**, *132*, 154104.
[52] N. Canning, R. J. Madix, *J. Phys. Chem.* **1984**, *88*, 2437–2446.
[53] a) R. G. Greenler, *J. Chem. Phys.* **1966**, *44*, 310–315; b) R. G. Greenler, D. R. Snider, D. Witt, R. S. Sorbello, *Surf. Sci.* **1982**, *118*, 415–428.
[54] a) B. Hagman, A. Posada-Borbón, A. Schaefer, M. Shipilin, C. Zhang, L. R. Merte, A. Hellman, E. Lundgren, H. Grönbeck, J. Gustafson, *J. Am. Chem. Soc.* **2018**, *140*, 12974–12979; b) T. Yang, T. Gu, Y. Han, W. Wang, Y. Yu, Y. Zang, H. Zhang, B. Mao, Y. Li, B. Yang, Z. Liu, *J. Phys. Chem. C* **2020**, *124*, 27511–27518.
[55] R. Bavisotto, R. Rana, N. Hopper, D. Olson, W. T. Tysoe, *Phys. Chem. Chem. Phys.* **2021**, *23*, 5834–5844.
[56] R. Bavisotto, R. Rana, N. Hopper, W. T. Tysoe, *Surf. Sci.* **2021**, *711*, 121875.

Manuscript received: June 11, 2021